An RKR-like inversion procedure for bound–continuum transition intensities

Mark S. Child, Hanno Essén,[a] and Robert J. Le Roy[b]

Departmnt of Theoretical Chemistry, University of Oxford, 1 South Parks Road, Oxford OX1 3TG, England
(Received 16 December 1982; accepted 17 February 1983)

A semiclassical RKR-like inversion procedure for determining a repulsive diatomic molecule potential energy curve from structured bound–continuum transition intensity data is derived and tested. The method presumes a knowledge of the (attractive) initial state potential well and of the energy and vibrational assignment of the absorbing or emitting level. Its application to a structured emission continuum of NaK observed by Breford and Engelke [Chem. Phys. Lett. **53**, 282 (1979)] yields a potential energy curve which is incompatible with other known properties of this system, a result which confirms the suggestion of Kato and Noda [J. Chem. Phys. **73**, 4940 (1980)] that the original assignment of the initial state for this spectrum is in error.

I. INTRODUCTION

The determination of repulsive diatomic molecule potential curves from bound–continuum transition intensities is a very old problem which has been attracting attention since the early days of quantum mechanics.[1] Over the years, work on it has usually been based on a wave mechanical description of the phenomenon, with most attention being focused on the problem of efficient and accurate evaluation of the overlap integrals between the oscillating bound and continuum wave functions.[2–13] Once a computational scheme was adopted, these overlap integrals would be evaluated for some trial potential energy and transition moment functions, and those trial functions varied until the synthetic spectrum agreed with experiment. In the early days, the simplifying approximations introduced in order to make the computations feasible limited the accuracy of potentials obtained in this way. However, modern computer technology and numerical methods removed the need for such approximations more than a decade ago, so that the accuracy of potentials and transition moment functions obtainable in this way is now mainly determined by the quality and extent of the experimental data.[13]

While bound–continuum absorption or emission intensities can in principle always be analyzed using the "exact" computational and fitting procedures referred to above, the more direct inversion procedure reported below is a complementary approach which offers some distinct advantages. The first of these is that it provides greater insight into the nature of the information contained in the experimental data. In particular, it distinguishes between the "phase" and "amplitude" information in the experimental spectrum and shows how the positions of the intensity extrema are determined by the shape of the continuum potential while the peak heights depend on the transition dipole function. The second advantage is that, as with any RKR-like inversion procedure, the present method requires no prior assumption about the analytical form of the potential or transition moment function. Finally, the computational effort required by this method is minimal.

The procedure described herein is based on Hunt and Child's uniform harmonic approximation for bound–free overlap integrals.[14,15] This approximation is reviewed and tested in Sec. II and show to be substantially more accurate than commonly used older overlap integral approximation methods.[1,12] The inversion procedure is derived in Sec. III and tested in Sec. IV by application to a synthetic spectrum generated from a model for the visible photodissociation continuum of Br_2. Its utility is further demonstrated in Sec. V where it is used to analyze a fluorescence emission continuum of NaK.[16]

II. THE UNIFORM HARMONIC APPROXIMATION FOR BOUND-CONTINUUM OVERLAP INTEGRALS

The phenomenon of interest is the absorption (or emission) of light of frequency $\nu = |E - E_v|/hc$ by a molecule initially in vibrational level v with energy E_v and inner and outer turning points a_2 and b_2, respectively, on the initial state potential energy curve $V_2(R)$, causing a transition to a continuum state at energy E with turning point $R_1(E)$ on the repulsive potential curve $V_1(R)$. This phenomenon is illustrated in Fig. 1 for the case of absorption from the $v = 5$ level of the ground ($X\ ^1\Sigma_g^+$) state of Br_2 into the continuum associated with the repulsive $^1\Pi_{1u}$ state.[6,13] The resulting calculated (exact quantal) absorption continuum is shown on the left-hand side of this diagram. As throughout this paper, the zero of energy is taken to be the energy E_v of the initial vibrational level. Note too that the present discussion applies equally well to absorption or emission, the only difference between them being that for the latter the energies E and $V_1(R)$ are negative (i.e., less than E_v).

The two essential conditions for the applicability of the present procedure are that $V_1(R)$ must be purely repulsive on the interval $a_2 \leq R \leq b_2$, and that at any final state energy E for which the turning point $R_1(E)$ lies between a_2 and b_2, there exists exactly one momentum-conserving transition point $R_x(E)$ lying be-

[a] Present address: Institute for Theoretical Physics, University of Stockholm, Vanadisvagen 9, S-11346 Stockholm, Sweden.

[b] Present and permanent address: Guelph-Waterloo Centre for Graduate Work in Chemistry, University of Waterloo, Waterloo, Ontario N2L 3G1, Canada.

 0021-9606/83/116732-09$02.10

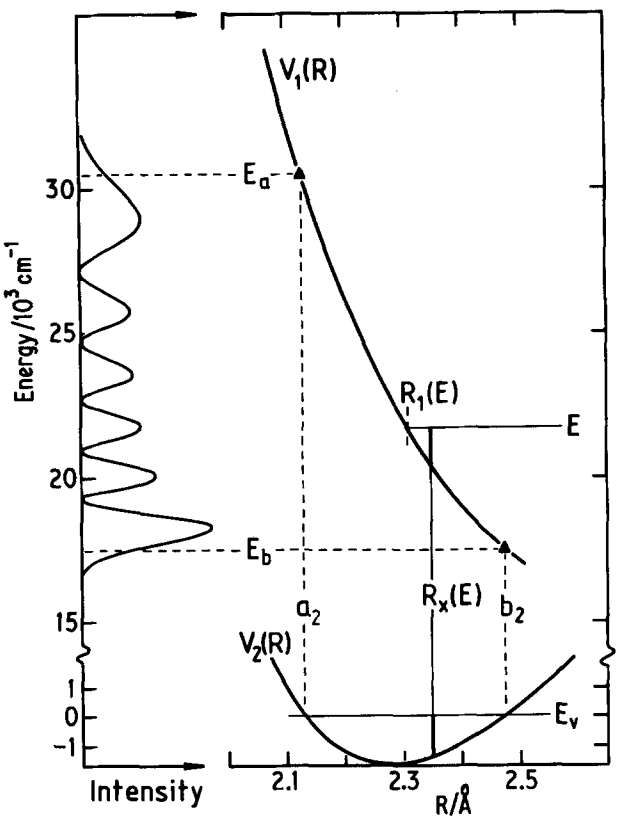

FIG. 1. Illustration of the phenomenon and defintion of variables for the $X\,^1\Sigma_g^+ \rightarrow {}^1\Pi_{1u}$ spectrum of Br_2.

tween $R_1(E)$ and b_2 which satisfies the criterion

$$E - V_1(R_x) = E_v - V_2(R_x) \ . \tag{1}$$

If this condition is not satisfied the transition intensity acquires a more complex interference structure[1,15,17] and the theory and inversion procedure used here is not valid.[18]

The present theory is based on Hunt and Child's[15] uniform harmonic approximation for the transition amplitude coupling a discrete and a continuum state

$$M_{vE} \equiv \int_0^\infty \Psi_{2v}(R) M(R) \Psi_{1E}(R)\, dR$$

$$\approx M(R_x)\,[\bar{\omega}/(u_x \Delta F_x)]^{1/2}\,[2v + 1 - \xi(E)^2]^{1/4} \phi_v(\xi(E)) \ , \tag{2}$$

where $\phi_v(\xi)$ is the vth harmonic oscillator wave function[19]

$$\phi_v(\xi) = [2^v v!\, \pi^{1/2}]^{-1/2} H_v(\xi) \exp(-\xi^2/2) \tag{3}$$

and its argument $\xi(E)$ is implicitly defined by the equation

$$\Delta(E) = (2\mu/\hbar^2)^{1/2} \left\{ \int_{R_1(E)}^{R_x(E)} [E - V_1(R)]^{1/2}\, dR + \int_{R_x(E)}^{b_2} [E_v - V_2(R)]^{1/2}\, dR \right\}$$

$$= -\xi(2v + 1 - \xi^2)^{1/2}/2 + (v + 1/2) \cos^{-1}[\xi/(2v+1)^{1/2}] \ , \tag{4}$$

where μ is the reduced mass. The constant $\bar{\omega}$ appearing in Eq. (2) is the classical bound state oscillation frequency for level v,

$$\bar{\omega} \equiv (\partial E_v/\partial v)/\hbar \tag{5}$$

and the quantities u_x and ΔF_x are defined by the properties of the two potential energy curves at the transition point R_x:

$$u_x = \{2[E - V_1(R_x)]/\mu\}^{1/2} \ , \tag{6}$$

$$\Delta F_x = [V_2'(R_x) - V_1'(R_x)] \ , \tag{7}$$

where primes denote differentiation with respect to R.

Note that the validity of Eq. (2) should not depend significantly on the nature of the $M(R)$ function as long as it does not undergo drastic nonlinear changes on a range comparable to the de Broglie wavelength associated with the $\Psi_{1E}(R)$ function. In the extreme case that this did occur, the present approach would not be appropriate. Note too that this "uniform harmonic approximation" *does not* assume that $\Psi_{2v}(R)$ can be accurately represented by a harmonic oscillator wave function, but rather maps the latter onto the former in a way which mimics the phase and amplitude behavior of the exact function.

The basis of the present procedure is Eq. (4), which maps M_{vE} onto the known function $\phi_v(\xi)$ by requiring the phase integral sum in the first line of this equation be equal to the uniform asymptotic approximation model for it given in the last line. It is readily shown that utilization of the JWKB approximation for the normalized function[20]

$$\phi_v(\xi) \simeq (2/\pi)^{1/2} [2v + 1 - \xi^2]^{-1/4} \sin[\Delta(E) + \pi/4] \tag{8}$$

reduces Eq. (2) to its well-known primitive semiclassical form[21]

$$M_{vE} \simeq M(R_x)(2\bar{\omega}/\pi u_x \Delta F_x)^{1/2} \sin[\Delta(E) + \pi/4] \ . \tag{9}$$

Equation (2) was tested by comparing its predictions with the results of exact (numerical) quantum mechanical calculations for the two model problems considered below. The first of these, modeled on the $X\,^1\Sigma_g^+ \rightarrow {}^1\Pi_{1u}$ absorption continuum of Br_2 (see Sec. IV),[6,13] is a case in which the repulsive potential supporting the continuum wave functions is much steeper than the repulsive branch of the bound state potential over the whole of the interval between the turning points of the latter. This is the optimum situation for the use of Eq. (2), and in this case its predictions are virtually indistinguishable from the quantal calculations.

The second test case is a model based on a continuum emission spectrum of NaK, which was initially identified as the $D\,^1\Pi \rightarrow a\,^3\Sigma^+$ transition (see Sec. V).[16] It provides a more critical test of Eq. (2) because for R_x values near a_2 the difference between the slopes of the initial and final state potentials ΔF_x becomes fairly small. Nevertheless, the comparison with quantal calculations seen in segments A and B of Fig. 2 is very gratifying. In particular, the positions of all but the two lowest-frequency (i.e., highest continuum state energy) maxima are correct to within 0.5% of the peak separation, while the errors in two remaining peak positions are only slightly larger. Similarly, except for the lowest frequency maxima, the peak heights obtained using Eq. (2) are correct to better than 1%, and the bulk of the error for the remaining points is probably largely due to the fact that ΔF_x is small there.

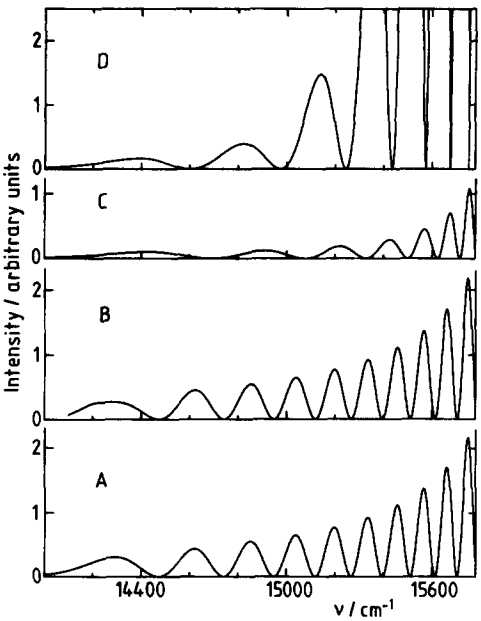

FIG. 2. Comparison of various methods for calculating bound–continuum transition intensities for the case of the NaK emission spectrum discussed in Sec. V: A—exact quantal calculation; B—uniform harmonic approximation of Eq. (2); C—Condon reflection approximation; D—Gislason's local Airy function approximation.

For the sake of comparison, Fig. 2 also contains plots of this same spectrum as predicted by the Condon reflection approximation (segment C)[1,2] and Gislason's local Airy function approximation (segment D).[12,13] The former approximates the continuum state wave function $\Psi_{1E}(R)$ by a delta function located at the turning point $R_1(E)$, while the latter approximates $\Psi_{1E}(R)$ by an Airy function and evaluates the overlap integral analytically after expanding the bound state wave function $\Psi_{2v}(R)$ in a Taylor series about $R_1(E)$. These two methods yield predictions which bear only a superfacial resemblance to the exact spectrum. While the Gislason method performs slightly better than the reflection approximation at low frequencies, it becomes completely unreliable at low continuum state energies where the slope of the final state potential at the classical turning point is relatively small. This behavior reflects the breakdown of the fundamental approximation underlying both of these methods, the requirement that the de Broglie wavelength of the bound state wave function be much longer than the oscillation period of the continuum wave function near its turning point. In general, this approximation will break down most readily for low continuum state energies and high-v bound state levels. Thus, these older approximation methods are even less reliable than was suggested by the discussion of Ref. 13 which considered only absorption by molecules in thermal equilibrium, a situation in which contributions from low-v states are dominant.

This virtually complete breakdown of the delta function[1-3] and Gislason[12] approximations provides a much more dramatic warning about the weakness of those procedures than was evident from previous studies.[13] It therefore appears that the uniform harmonic approximation of Eq. (2) is probably the most reliable approximate method for evaluating bound–continuum matrix elements. Its main weaknesses are that it becomes unstable when the potential slope difference ΔF_x approaches zero, and that it is restricted to continuum state energies for which $a_2(v) \leq R_1(E) \leq b_2(v)$. However, in practice these are not very severe limitations.

III. THE INVERSION PROCEDURE

The inversion procedure has two steps. The first of these is the determination of the energy dependence of $\xi(E)$, and hence of $\Delta(E)$, by mapping the intensity maxima and/or minima of the observed spectrum onto the positions of the extrema and nodes of the harmonic oscillator functions $\phi_v(\xi)$. The second step is the determination of the repulsive potential $V_1(R)$ from this knowledge of $\Delta(E)$. Upon completion of this inversion, it is also possible to extract the radial dependence of $M(R)$ from a knowledge of the amplitudes of the intensity maxima. Note that application of this procedure requires a prior knowledge of the bound state potential $V_2(R)$ and the vibrational quantum number v of the initial state. It also presumes that the observed intensity maxima have been correctly assigned to the appropriate extrema of $\phi_v(\xi)$.

For $v = 1$–13, Table I lists the ξ values associated with the maxima of the harmonic oscillator probability density $[\phi_v(\xi)]^2$; the associated minima correspond to the

TABLE I. Positions ξ of the extrema of the harmonic oscillator functions $\phi_v(\xi)$ for $v = 1$ to 13.

$v=1$	±1.000 000						
2	0.000 000	±1.581 139					
3	±0.602 114	±2.034 074					
4	0.000 000	±1.074 613	±2.417 686				
5	±0.476 251	±1.475 241	±2.756 238				
6	0.000 000	±0.881 604	±1.828 611	±3.062 508			
7	±0.406 782	±1.239 870	±2.147 928	±3.344 197			
8	0.000 000	±0.767 093	±1.563 978	±2.441 238	±3.607 717		
9	±0.361 030	±1.093 513	±1.861 876	±2.713 869	±3.852 560		
10	0.000 000	±0.688 554	±1.393 823	±2.138 862	±2.969 559	±4.085 357	
11	±0.327 945	±0.990 182	±1.673 236	±2.398 674	±3.211 048	±4.306 716	
12	0.000 000	±0.630 249	±1.271 027	±1.935 443	±2.644 063	±3.440 417	±4.518 164
13	±0.302 575	±0.911 931	±1.534 724	±2.183 173	±2.877 123	±3.659 285	±4.720 912

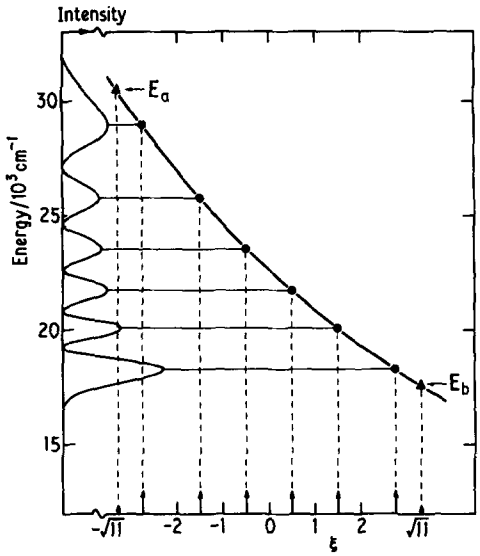

FIG. 3. For the Br_2 model problem of Sec. IV in which the initial level corresponds to $v = 5$, determination of the function $\xi(E)$ from the observed intensity extrema positions.

nodes of $\phi_v(\xi)$ and are available elsewhere as the integration mesh points for the Gauss–Hermite quadrature formula.[22] The energy dependence of $\xi(E)$ is defined by associating these ξ values with the appropriate maxima and minima of the observed transition intensity. For the $v = 5$ model problem of Fig. 1 (see section IV), this procedure is illustrated in Fig. 3 where the absorption intensity as a function of energy is plotted along the vertical axis and the ξ values associated with the maxima of $[\phi_5(\xi)]^2$ are indicated by arrows on the horizontal axis. Interpolation over the six points associated with these intensity maxima clearly defines a smooth $\xi(E)$ function.

On a plot such as Fig. 3 it is a very straightforward procedure to extrapolate to determine the energies associated with the harmonic oscillator function turning points at $\xi = +(2v+1)^{1/2}$ and $-(2v+1)^{1/2}$. Consideration of Eq. (4) shows that these ξ values correspond to $\Delta(E) = 0$ and $(v+1/2)\pi$, respectively, and hence that the associated energies E_b and E_a are those for which the final state turning point $R_1(E)$ coincides with the known initial state turning points b_2 and a_2, respectively. Thus, extrapolation of $\xi(E)$ to $\xi(E_a) = -(2v+1)^{1/2}$ and $\xi(E_b) = +(2v+1)^{1/2}$ determines the two points (triangular points in Fig. 3) $V_1(b_2) = E_b$ and $V_1(a_2) = E_a$ which bound the range of final state potential energy accessible to the present procedure.

Once the smooth function $\xi(E)$ is determined from the mapping described above, its energy derivative may be obtained and used to define the function obtained upon differentiation of Eq. (4):

$$d\Delta/dE = -(2v+1-\xi^2)^{1/2}(d\xi/dE)$$

$$= \tfrac{1}{2}(2\mu/\hbar^2)^{1/2}\int_{R_1(E)}^{R_x(E)} dR/[E - V_1(R)]^{1/2} . \qquad (10)$$

The key to the derivation is then to apply an Abelian transformation to Eq. (10) by defining the integral

$$I(E) = \int_{E_b}^{E} dE'\,(d\Delta/dE')/[E-E']^{1/2} \qquad (11)$$

and substituting Eq. (10) into it, to obtain

$$I(E) = \tfrac{1}{2}(2\mu/\hbar^2)^{1/2}\int_{E_b}^{E} dE'\left(\int_{R_1(E')}^{R_x(E')} dR/\{(E-E')\times[E'-V_1(R)]\}^{1/2}\right) . \qquad (12)$$

By breaking the range of integration for R into two subintervals,

$$[R_1(E'), R_x(E')] = [R_1(E'), b_2] - [R_x(E'), b_2] , \qquad (13)$$

this integral may be divided into two parts:

$$I(E) = I_1(E) - I_2(E) . \qquad (14)$$

The domains for the resulting double integrations may be seen in Fig. 4. On interchanging the order of integration, the first of these integrals reduces to a simple linear function of the desired turning points $R_1(E)$:

$$I_1(E) = \tfrac{1}{2}(2\mu/\hbar^2)^{1/2} \times \int_{R_1(E)}^{b_2} dR \int_{V_1(R)}^{E} dE'/\{(E-E')[E'-V_1(R)]\}^{1/2}$$

$$= (\pi/2)(2\mu/\hbar^2)^{1/2}[b_2 - R_1(E)] . \qquad (15)$$

This manipulation is essentially the same as those at the core of other semiclassical inversion procedures,[23] including the RKR method of bound state spectroscopy.[24] Application of this same procedure to $I_2(E)$ yields the result

$$I_2(E) = \tfrac{1}{2}(2\mu/\hbar^2)^{1/2} \times \int_{R_x(E)}^{b_2} dR\left(\int_{E_x}^{E} dE'/\{(E-E')[E'-V_1(R)]\}^{1/2}\right.$$

$$= \tfrac{1}{2}(2\mu/\hbar^2)^{1/2}\int_{R_x(E)}^{b_2} dR(\pi/2 + \arcsin \times\{1 - 2[E_v - V_2(R)]/[E - V_1(R)]\}) , \qquad (16)$$

where $E_x(R) = V_1(R) + E_v - V_2(R)$ is defined by Eq. (1) as the energy for which $R_x(E) = R$. Combining Eqs. (11)–

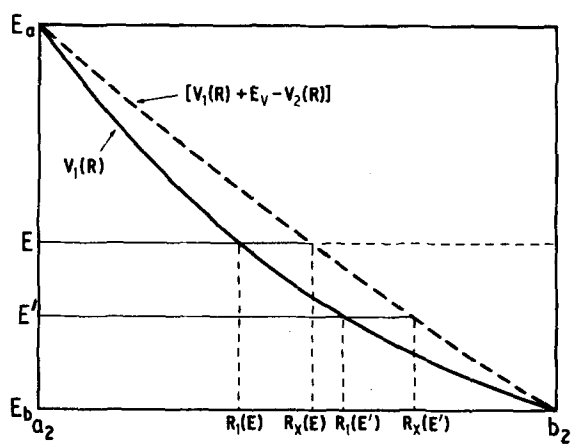

FIG. 4. Domains of integration associated with evaluation of $I(E)$ using the partitioning of Eqs. (13)–(16).

(16) then yields the final result of this derivation:

$$R_1(E) = \tfrac{1}{2}[b_2 + R_x(E)] - [2/\pi(2\mu/\hbar^2)^{1/2}] \times \int_{E_b}^{E} dE'\,(d\Delta/dE')/[E - E']^{1/2} - (1/\pi)\int_{R_x(E)}^{b_2} dR \arcsin\{1 - 2[E_v - V_2(R)]/[E - V_1(R)]\}\,. \tag{17}$$

The first integral on the right-hand side of Eq. (17) is readily evaluated[25] from the experimentally determined energy dependence of $\xi(E)$ and $\Delta(E)$. On the other hand, prior knowledge of the *desired* potential $V_1(R)$ on the interval $R_x(E) \le R \le b_2$ is required to define both the value of $R_x(E)$ [from Eq. (1)] and the integrand of the remaining integral. However, for any $E > E_b$, $R_x(E)$ lies *between* b_2 and $R_1(E)$ (see Fig. 1). Thus, once $V_1(R)$ is known on some interval $[R^*, b_2]$ for any $R^* < b_2$, Eq. (17) may be used to extend the region in which $V_1(R)$ is known inward to $R_1(E_x(R^*))$. Repetition of this procedure will then progressively extend this interval all the way to the initial state inner turning point, $R = a_2$.

The only problem remaining is that of determining $V_1(R)$ on the initial interval $[R^*, b_2]$. Fortunately, for R^* (and hence R_x) close to b_2, the second integral in Eq. (17) is much smaller than the first one. As a result, Eq. (17) may be used iteratively to determine $R_1(E_x(R^*))$ in a self-consistent fashion starting from virtually any plausible initial estimate of its value. For the model problems considered below, this initialization procedure converged in very few cycles, independent of the choice of this initial value or of the initial energy step.[26] Moreover, this convergence may be facilitated by using the known behavior of $\xi(E)$ at the end points of the range $[E_b, E_a]$ to yield values of the first derivatives of $V_1(R)$ at those points. In particular, in the limit when $E \to E_b$, $V_1(R)$ and $V_2(R)$ become exactly linear on the interval $[R_1(E), R_x(E)]$ and Eq. (10) yields the expression (where primes denote differentiation with respect to R):

$$V_1'(b_2)[1 - V_1'(b_2)/V_2'(b_2)]^{1/2} = -\{2(\hbar^2/2\mu)(2v+1)^{1/2}[-d\xi/dE]^3\}^{-1/2}\,, \quad E = E_b\,, \tag{18}$$

which may be readily solved (numerically) for $V_1'(b_2)$. An expression exactly analogous to Eq. (18) may be similarly obtained for the potential derivatives at the inner turning point $R = a_2$.

As described above, the inversion procedure starts at the extrapolated point $E = E_b = V_1(b_2)$ and generates turning points $R_1(E)$ on $V_1(R)$ at a sequence of increasing energies until the inner turning point a_2 at the extrapolated point $E_1 = V_1(a_2)$ is reached. The errors in the resulting potential are expected to be quite small, except perhaps near the inner end of this range $R_1(E) \to a_2$ where the increasing magnitude of the potential slope and proximity to the end of the range may sometimes amplify the effect of cumulative error in the representation of the phase information in the data. However, the fact that the end point $R_1(E_a) = a_2$ is already known (fairly accurately) from extrapolation of the $\xi(E)$ function, together with the constraint that the resulting potential (including this end point) must always have positive curvature, allows the calculations to be truncated before this error introduces any problem. Interpolation between the calculated $R_1(E)$ points and the known point at $R_1(E_a)$ then yields a smooth potential on the whole interval.

A technical point deserving comment here concerns the numerical procedures used for evaluating the integrals appearing in Eq. (17). The integrand of the first integral clearly has an $x^{-1/2}$ singularity at the upper end of its range of integration and goes to zero as $x^{1/2}$ at the lower limit, while the integrand in the second integral dies off like $x^{1/2}$ at *both* ends of the range of integration. These integrals should therefore be evaluated using the Gauss–Tchebyshev quadrature procedures which take proper account of this limiting behavior.[27] In both cases, 16 point quadratures provide more than enough accuracy for present purposes.

In practice, the main source of error for the inversion procedure is uncertainties in the measured positions of the intensity extrema. Thus, appropriate steps should be taken to ensure that the function $(d\Delta/dE')$ is a smooth function of energy. In the present work this smoothing was accomplished by fitting the input phase information to polynomials in ξ and using numerical inversion of the resulting expression to yield the desired phase derivative values.

An annotated listing of a fortran program utilizing the above inversion procedure may be obtained from the authors on request.

IV. TESTING THE METHOD ON THE $X\ ^1\Sigma_g^+(v=5) \to\ ^1\Pi_{1u}$ ABSORPTION CONTINUUM OF Br_2

As a first test, the above method was applied to synthetic data for visible absorption from the $v = 5$ level of the $X\ ^1\Sigma_g^+$ state of Br_2 into continuum levels of the $^1\Pi_{1u}$ state sharing the same dissociation limit. The potential energy curves and spectrum from this case are sketched in Fig. 1. The synthetic spectrum was generated by performing exact quantum mechanical calculations using the potential energy curves of Ref. 13; the X-state potential was represented by the turning points of Barrow *et al.*[28] while the $^1\Pi_{1u}$ state potential was defined by the function (with energies in cm^{-1} and lengths in Å)[13]

$$V_1(R) = 7654 \times \exp[-4.6368(R - 2.3) - 0.879(R - 2.3)^2] \tag{19}$$

expressed relative to the X-state dissociation threshold. The only additional parameter required to define this problem is the binding energy of the absorbing $v = 5$ X-state level, 14311.38 cm^{-1}. For the sake of simplicity, this model spectrum was generated with $M(R) \equiv 1$ and with the explicit frequency dependence omitted from the absorption coefficient expression.[13]

The input data taken from this synthetic spectrum were the energies of the six absorption intensity maxima: 18257.8, 20088.2, 21773.2, 23609.8, 25790.9, and 28969.6 cm^{-1}. In Fig. 3 these points are plotted vs the appropriate ξ values taken from Table I. Extrapolation at the ends of this range using $(N-1)$th order poly-

nomials fitted to the first/last N points yielded E_a estimates of 30 486–30 495 cm^{-1} and E_b estimates of 17 562–17 574 cm^{-1}, for $N = 3$–6. These extrapolated values for both end points lie slightly below the true points on the model-problem potential: $V_1(a_2) = 30\,614$ cm^{-1} and $V_1(b_2) = 17\,591$ cm^{-1}. Thus, while these extrapolations are potentially one of the main sources of error in the present method, in this case the resulting discrepancies are small relative to the variation of the potential across the range under consideration.

Since the input intensity information for this case was numerically generated, it required no smoothing. Values of $\xi(E)$ and $d\xi/dE$ required in the evaluation of the first integral in Eq. (17) [see Eq. (10)] were therefore determined by piecewise polynomial interpolation over the six intensity-maxima points; the results obtained were essentially unchanged when the order of the polynomials used in this ξ interpolation was varied from 2 to 5. In determining $R_x(E)$ and evaluating the second integral in Eq. (17), eight-point piecewise polynomials were used to interpolate over the given initial-state turning points, while four-point piecewise interpolation was performed for $V_1(R)$. As above, the results obtained were insensitive to the order of the interpolating polynomial as long as it was not too small.

For the Br_2 model problem, the reliability of the present method is illustrated by Fig. 5. The solid curve there corresponds to the differences between the values of $R_1(E)$ generated by the inversion procedure and the corresponding turning points of the "true" potential used to generate the synthetic spectrum. The dashed curve shows how the cumulative errors mentioned above tend to exaggerate these discrepancies in the limit when $R_1(E) - a_2$ if the requirement that $V_1(R)$ be well behaved (i.e., have a positive second derivative) is not used to truncate the calculation. The errors at the ends of the range are simply the errors associated with the extrapolation beyond the input phase information to locate the energies corresponding to $\xi = \pm(2v+1)^{1/2}$.

In conclusion, the maximum errors in the Br_2 turning points $R_1(E)$ yielded by the present inversion procedure

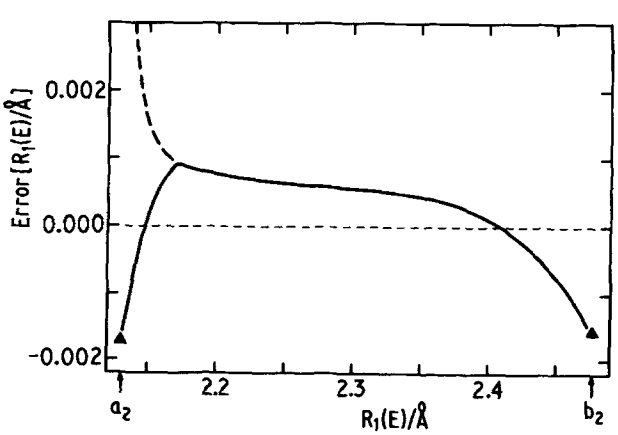

FIG. 5. Errors in the turning points $R_1(E)$ of the potential obtained on applying the present inversion procedure to the synthetic Br_2 model-problem data.

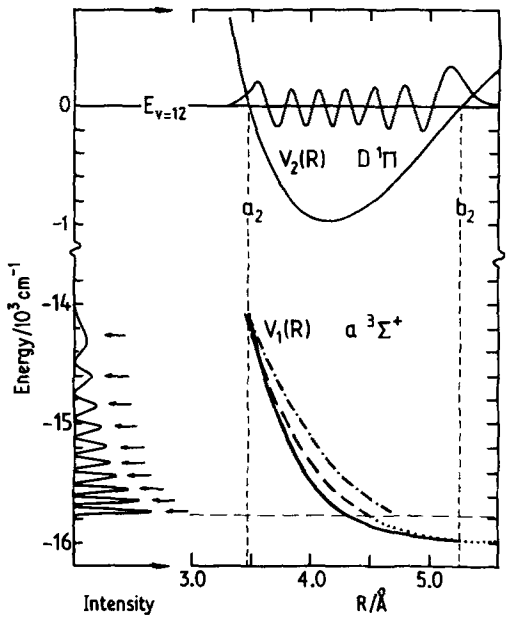

FIG. 6. Model associated with the original assignment of the observed (Ref. 16) structured emission continuum of NaK.

are less than 0.5% of the turning point range considered, $b_2 - a_2 \simeq 0.35$ Å. This is a very gratifying result, as these discrepancies would not even be discernable on the scale of the plot shown in Fig. 1.

V. APPLICATION TO A STRUCTURED EMISSION CONTINUUM OF NaK

A. Application of the inversion procedure

A more challenging test of the present method is provided by the structured continuum emission into the $a\,^3\Sigma^+$ state of NaK which Breford and Engelke observed subsequent to their laser excitation of the $v = 12$ level of the $D\,^1\Pi$ state.[16] It has since been proposed that the observed emission actually originates in the near resonant $v = 13$ vibrational level of the perturbing $d\,^3\Pi_1$ triplet state.[29] However, the present study first examines the implications of the original[16] identification of $D\,^1\Pi(v = 12)$ as the emitting level.

The model implied by this assignment of the observed spectrum is summarized in Fig. 6. The excited $D\,^1\Pi$ state has been studied through absorption from the ground $X(^1\Sigma^+)$ state,[30] and its potential energy curve determined using the RKR inversion procedure. The resulting inner and outer turning points of the $v = 12$ D-state level are $a_2 = 3.463\,67$ Å and $b_2 = 5.264\,75$ Å. The $a\,^3\Sigma^+$ state potential which supports the final-state continuum levels has a shallow van der Waals well and dissociates at the same limit as does the ground state,[16,31,32] at an energy some 15 778.4 cm^{-1} below the $v = 12$ D-state level.

The existence of discrete emission into the bound levels of the $a(^3\Sigma^+)$-state potential well complicates the inversion problem. In particular, this discrete structure accounts for the high frequency end of the emission spectrum, so that only 10 of the 13 possible intensity maxima lie in the continuum region above the $a(^3\Sigma^+)$-

TABLE II. Frequencies, amplitudes,[a] and ξ values[b] associated with the $D\,^1\Pi(v=12) \rightarrow a\,^3\Sigma^+$ assignment of the structured emission continuum of NaK.

ν/cm^{-1}	Amplitude	ξ	ν/cm^{-1}	Amplitude	ξ
14 278	36	−4.518 164	15 351	76	−0.630 249
14 426	0	−3.889 725	15 389	0	−0.314 240
14 616	40	−3.440 417	15 454	82	0.0
14 753	0	−3.020 637	15 501	0	0.314 240
14 860	40	−2.644 063	15 564	121	0.630 249
14 940	0	−2.279 507	15 603	0	0.947 788
15 044	50	−1.935 443	15 652	142	1.271 027
15 117	0	−1.597 683	15 696	0	1.597 683
15 211	62	−1.271 027	15 743	163	1.935 443
15 269	0	−0.947 788	(15 977[c])	···	5.0

[a]Frequencies and heights (arbitrary units) of observed intensity extrema taken from an expanded version of Fig. 3 of Ref. 16.
[b]Zeros, extrema and turning points of $\phi_{12}(\xi)$.
[c]Determined from known RKR potential at b_2.

state dissociation limit. In the absence of additional information, this lack of knowledge of the intensity extrema associated with the outermost part of the initial state wave function would make the extrapolation to the outer phase end point $\xi(E_b) = +(2v+1)^{1/2}$ relatively long, leading to increased uncertainty in the extrapolated value of $E_b = V_1(b_2)$. However, a reliable value of this quantity is readily obtained by interpolating over the RKR turning points for the bound portion of the a-state curve obtained from an analysis of the discrete portion of this emission spectrum.[31] This approach yielded the energy $E_b = V_1(b_2) = -15\,976.9\ \mathrm{cm}^{-1}$ (relative to the emitting state) and derivative $V_1'(b_2) = -52\ \mathrm{cm}^{-1}\,\text{Å}^{-1}$ for the potential at $\xi = +(2v+1)^{1/2} = 5$. Use of the latter quantity in Eq. (18) also yields a value for the phase derivative $d\xi/dE$ at this end point.

In principle, the envelope of intensities of the discrete transitions in the adjacent bound–bound portion of the emission spectrum could be used to define additional values of the $\xi(E)$ function at energies below the final state dissociation threshold. In the present case two additional intensity maxima and three intensity minima could be clearly assigned in this way.[16] However, the accurate knowledge of E_b and of the lower portion of $V_1(R)$ provided by the RKR potential makes this unnecessary, so the present analysis utilized only the intensity extrema lying above the a-state dissociation limit.

A second complication is the fact that the emission intensity is actually proportional to

$$I_{vE} = \nu^4 |M_{vE}|^2 \tag{20}$$

so that the positions of the observed intensity maxima will in general be affected by both the frequency factor ν^4 and the R dependence of the transition dipole [see Eq. (2)]. One way around this problem would be to base the inversion procedure only on the intensity minima, as their positions are not affected by these factors. However, this would increase the length of the extrapolations to determine the energy $E_a = V_1(a_2)$ corresponding to $\xi(E) = -(2v+1)^{1/2}$ and make the resulting value less reliable, so this approach is not desirable. Fortunately, these peak position shifts are usually fairly small and may be corrected for iteratively. To this end, the shifts may initially be neglected and the inversion procedure used to obtain initial estimates of $V_1(R)$ and $M(R)$. Comparison of synthetic spectra generated from this potential with and without inclusion of the ν^4 and transition moment factors then yields estimates of the shifts. Subtracting these displacements from the observed peak positions then yields "corrected" input data, for use in the inversion procedure. In the present problem, only the two lowest-frequency maxima shifted significantly, the first by 24 cm^{-1} and the second by 5 cm^{-1}, and taking account of these displacements had little effect on the resulting $V_1(R)$ and $M(R)$ functions.

The observed positions and amplitudes of the 19 lowest frequency (highest E) intensity extrema in the NaK emission spectrum are listed in Table II,[33] together with the ξ values associated with the assignment of this spectrum as emission from the D-state $v = 12$ level. Also shown there is the energy $E_b = V_1(b_2)$, corresponding to $\xi = +5$, determined from the a-state RKR potential. In the inversion, the $E(\xi)$ function was represented by a third-order polynomial fitted to the 19 experimental points and constrained to be consistent with both the known point $E_b = E(\xi = +5)$ and the phase derivative at this point, defined by Eq. (18).

The repulsive portion of the $a(^3\Sigma^+)$-state potential obtained using the present method is plotted as a solid curve in Fig. 6. The validity of the method is demonstrated by the fact that the positions of the intensity extrema of a spectrum calculated from this potential (intensity curve in Fig. 6) agree extremely well with the smoothed (by the polynomial fit) input peak positions (denoted by arrows in this figure). As can be seen from Eq. (2), the transition dipole function values $M(R_x(\nu_{max}))$ may be determined by comparing the observed peak heights with values calculated from Eqs. (2) and (20) while assuming $M(R) = 1$:

$$M(R_x(\nu_{max})) = [I_{obs}(\nu_{max})/I^{M=1}_{calc}(\nu_{max})]^{1/2}\ . \tag{21}$$

The results obtained in this way, plotted in Fig. 7, are well represented by the linear function (for R in Å):

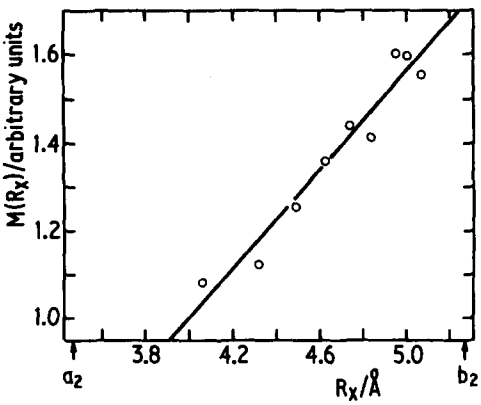

FIG. 7. Transition dipole function for NaK obtained from Eq. (21) for the $v = 12\, D(^1\Pi)$-state assignment of the emitting level.

$$M(R) = M_0[1 + 0.56(R - 4.0)]. \quad (22)$$

The net result of the inversion procedure is then summarized in segment (a) of Fig. 8 where the calculated spectrum implied by the inverted potential and transition moment function (solid curve) is compared to the positions (smoothed) and heights of the observed intensity maxima (vertical bars). The agreement seen there provides convincing evidence of the reliability of the present procedure.

For the sake of comparison, Fig. 6 also contains a plot of the final state potential implied by the reflection or delta-function approximation (dot–dashed curve). The large differences between it and the present inverted potential (solid a-state curve) reaffirms the conclusions implied by Fig. 2, that the delta-function approximation is grossly inadequate for this system.

B. Physical significance of the results

It is clear that the present procedure has successfully inverted the Breford–Engelke data to yield a repulsive wall for the $a(^3\Sigma^+)$ state potential. However, the discrepancy between the lower portion of this inverted potential (solid a-state curve in Fig. 6) and the inner wall of the RKR potential for this state (dotted curve) raises serious doubts about the physical significance of this result. In particular, the radial displacement of the inner wall of this potential by up to 0.15 Å seems much too large to be attributable to error in the RKR potential or in the molecular constants from which it was obtained.

To clarify this point and test further the sensitivity of the emission spectrum to small changes in the repulsive potential, the spectrum was recalculated[34] using the modified repulsive potential (energies in cm^{-1} and lengths in Å)

$$V_1(R) = -16090.5 + 755.25 \times \exp[-1.73(R - 4.0)] \quad (23)$$

whose parameters were chosen so that it would both smoothly join the upper end of the RKR curve and yield approximately the correct position for the intensity maximum at lowest frequency. This function is shown as a dashed curve in Fig. 6, and the corresponding predicted emission spectrum is plotted in segment (b) of Fig. 8. It is immediately clear that relatively small displacements from the present inverted potential (solid curve in Fig. 6) completely destroys the agreement between the calculated and observed high frequency spectrum.

It therefore seems clear that a repulsive wall for the $a(^3\Sigma^+)$ state which explains the structured emission continuum of Ref. 16 in terms of emission from the $v = 12$ level of the $D(^1\Pi)$ state is incompatible with the a-state RKR curve of Breford and Engelke.[31] The two possible explanations of this inconsistency are error in the RKR portion of the $a(^3\Sigma^+)$ potential curve or error in the assignment of the emitting state as the $v = 12$ of the $D(^1\Pi)$ state. The latter seems the more likely. This conclusion was independently reached in Ref. 29 on the basis of an analysis of the line intensities in the discrete portion of the emission spectrum. Those authors proposed that the emitting level be reassigned as $v = 13$ of a potential for the $d(^3\Pi_1)$ state, and they devised a d-state potential for which the calculated continuum and discrete structure and intensities agreed with experiment. However, since no independent information is available for the $d(^3\Pi_1)$ state we could not apply the present inversion procedure to this assignment.

VI. DISCUSSION AND CONCLUSIONS

The results presented in Secs. IV and V clearly show that the present inversion procedure can readily extract a unique and reasonably accurate potential curve and transition moment function from appropriate experimental data. Moreover, the computer program required is fairly simple and is extremely cheap to use; for example, generating 22 points on the inverted $a(^3\Sigma^+)$ potential curve of Fig. 6 cost less than 3 s on a fairly slow main frame computer (an IBM 4341).

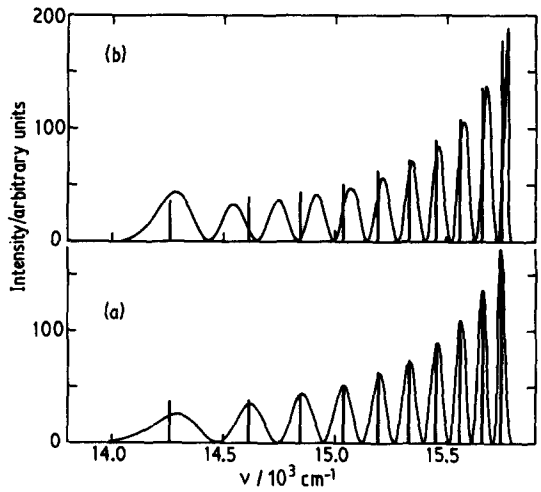

FIG. 8. Comparison with observed intensity maxima (vertical bars) of NaK emission spectra generated: (a) from the transition dipole and a-state potential (solid curve in Fig. 6) yielded by the present inversion procedure, and (b) from a modified a-state potential (dashed curve in Fig. 6) constrained to join the innermost RKR turning points.

In both of the sample applications described above, the rotational quantum number was equal to zero. However, this is in no way required by the present method, and emission or absorption by a discrete high-J level would be treated in exactly the same manner described above except that the two potentials $V_1(R)$ and $V_2(R)$ would include appropriate centrifugal distortion terms $J(J+1)\hbar^2/2\mu R^2$. An apparent difficulty is the fact that the given initial state usually emits/absorbs into states corresponding to more than one J value. However, for normal "symmetric" selection rules of $\Delta J = \pm 1$, or even $\Delta J = \pm 2$, the positions of the intensity extrema of the resulting spectrum would not differ significantly from those associated with a pure Q-branch ($\Delta J = 0$) spectrum, so treating such data as a Q-branch spectrum should introduce negligible errors. More serious difficulties arise if the discrete initial state absorbs or emits from a distribution of J sublevels. If this occurs, it would be necessary to attempt to associate the resulting spectrum with some effective or average initial J.

For the NaK system, the present analysis clearly confirms the conclusion of Ref. 29 that the repulsive curve implied by the $v = 12$ $D(^1\Pi)$-state assignment of the emitting level is incompatible with the RKR curve for the bound portion of the a state. As an alternate approach to this problem, it appears that a modified version of the present procedure could be combined with assumed knowledge of the repulsive part of the $a(^3\Sigma^+)$ state to yield the bound potential supporting the discrete emitting level. This method will be discussed in a future publication.[35]

ACKNOWLEDGMENTS

We are deeply indebted to Professor W. C. Stwalley whose perceptive comments have led to substantial improvements in this manuscript. In addition, R. J. LeRoy is grateful to the John S. Guggenheim Memorial Foundation for the award of a Fellowship which brought him to Oxford and allowed him to participate in this work, while H. Essén in indebted to the Royal Society of London for the award of a European Science Exchange Fellowship which permitted him to undertake this project.

[1](a) J. Franck, Trans. Faraday Soc. **21**, 536 (1925); (b) E. U. Condon, Proc. Natl. Acad. Sci. U.S.A. **13**, 462 (1927).
[2]E. U. Condon, Phys. Rev. **32**, 858 (1928).
[3]E. C. G. Stueckelberg, Phys. Rev. **42**, 518 (1932).
[4]G. E. Gibson, O. K. Rice, and N. S. Bayliss, Phys. Rev. **44**, 193 (1933).
[5]A. S. Coolidge, H. M. James, and R. D. Present, J. Chem. Phys. **4**, 193 (1936).
[6]N. S. Bayliss, Proc. R. Soc. London Ser. A **158**, 551 (1937).
[7]P. Sulzer and K. Wieland, Helv. Phys. Acta **25**, 653 (1952).
[8]G. H. Dunn, Phys. Rev. **172**, 1 (1968).
[9]R. O. Doyle, J. Quant. Spectrosc. Radiat. Transfer 8, 1555 (1968).
[10]A. C. Allison, A. Dalgarno, and N. W. Pasachoff, Planet. Space Sci. **19**, 1463 (1971).
[11]K. M. Sando, Mol. Phys. 23, 413 (1972)..
[12]E. A. Gislason, J. Chem. Phys. 58, 3702 (1973).
[13]R. J. LeRoy, R. G. Macdonald, and G. Burns, J. Chem. Phys. **65**, 1485 (1976).
[14]M. S. Child, Mol. Phys. **35**, 759 (1978).
[15]P. M. Hunt and M. S. Child, Chem. Phys. Lett. **58**, 202 (1978); Note that Eq. (5) of this paper should contain the additional factor $M(R_x)(\pi/2)$.
[16]E. J. Breford and F. Engelke, Chem. Phys. Lett. 53, 282 (1978).
[17]A. Dalgarno, G. Herzberg, and T. L. Stephens, Astrophys. J. **162**, L49 (1979).
[18]An analogous uniform approximation for the matrix elements for cases which do not satisfy this condition was reported in Ref. 15. See also: H. Krüger, Theor. Chim. Acta **51**, 311 (1979).
[19]M. Abramowitz and I. A. Stegun, *Handbook of Mathematical Functions* (Dover, New York, 1968).
[20]See Eqs. 19.10.10 and 19.13.1 of Ref. 19..
[21]L. D. Landau and E. M. Lifshitz, *Quantum Mechanics*, 2nd ed. (Pergamon, New York, 1965), p. 164.
[22]See Table 25.10 of Ref. 19.
[23](a) O. B. Firsov, J. Exp. Theor. Phys. 24, 279 (1953); (b) M. S. Child, J. Mol. Spectrosc. 33, 487 (1970).
[24]See, e.g., R. J. Le Roy, in *Semiclassical Methods in Molecular Scattering and Spectroscopy*, edited by M. S. Child (Reidel, Dordrecht, 1980, p. 109.
[25]Using Eq. 25.4.43 of Ref. 19.
[26]This was verified for slopes differing from the upper bound value of $(E_a - E_b)/(a_2 - b_2)$ by a factor of $2^{\pm 1}$, and for initial energy steps $[E_x(R^*) - E_b]$ ranging from 1 to 50 cm^{-1}.
[27]The first integral should be evaluated using Eq. 25.4.43 from Ref. 19 and the second on using its Eq. 25.4.41.
[28]R. F. Barrow, T. C. Clark, J. A. Coxon, and K. K. Yee, J. Mol. Spectrosc. 51, 428 (1974).
[29]H. Katô and C. Noda, J. Chem. Phys. **73**, 4940 (1980).
[30]M. M. Hessel and S. Giraud (unpublished).
[31]E. J. Breford and F. Engelke, J. Chem. Phys. **71**,1994 (1979).
[32]D. Eisel, D. Zevgolis, and W. Demtröder, J. Chem. Phys. **71**, 2005 (1979).
[33]E. J. Breford (private communication, 1979).
[34]This calculation was performed quantum mechanically with $M(R)$ defined by Eq. (22).
[35]R. J. Le Roy, R. Van Fleet, and M. S. Child (unpublished).